Chinese Journal of Structural Chemistry

ARTICLE

Pyrene-benzothiadiazole-based Polymer/CdS 2D/2D Organic/Inorganic Hybrid S-scheme Heterojunction for Efficient Photocatalytic H_2 Evolution

Ruiqi Gao[1+], Huan He[1+], Junxian Bai[1], Lei Hao[1], Rongchen Shen[1*], Peng Zhang[2], Youji Li[3] and Xin Li[1*]

[1]*Institute of Biomass Engineering, Key Laboratory of Energy Plants Resource and Utilization, Ministry of Agriculture and Rural Affairs, South China Agricultural University, Guangzhou 510642, China*

[2]*State Centre for International Cooperation on Designer Low-Carbon & Environmental Materials (CDLCEM), School of Materials Science and Engineering, Zhengzhou University, Zhengzhou 450001, China*

[3]*College of Chemistry and Chemical Engineering, Jishou University, Jishou* 416000, *Hunan, China*

ABSTRACT Nowadays, conjugated polymers have garnered numerous attention as a new class of organic photocatalysts due to their tunable electronic properties, low cost, excellent stability and sufficient light-absorption performance. In particular, pyrene-benzothiadiazole-based conjugated polymer (PBBP) has been considered to be a new type of conjugated polymers for photocatalytic H_2 evolution. However, the poor charge separation seriously limits its practical application in H_2 evolution. In this work, a PBBP-based polymer/CdS 2D/2D organic/inorganic S-scheme heterojunction photocatalyst with a strong internal electric field is, for the first time, prepared for efficient photocatalytic hydrogen evolution. The pyrene-benzothiadiazole-based conjugated polymers (PBBP) are synthesized by the Suzuki-Miyaura reactions. Then, the hybrid heterojunction photocatalysts are fabricated by coupling CdS with it through the ultrasonic mixing method. As a result, the highest H_2-production rate of 15.83 mmol h^{-1} g^{-1} is achieved on 20% PBBP/CdS composite under visible-light irradiation, nearly 2.7 times higher than that of pure CdS. The apparent quantum efficiency (AQE) of 20% PBBP/CdS composite could reach 8.66% at λ = 420 nm. The enhanced activity could be attributed to the construction of S-scheme heterojunction, which accelerates the recombination of carriers with weaker redox ability and maintains the strong reducibility of electrons in CdS. This work provides a protocol for pyrene-benzothiadiazole-based conjugated polymers to prepare S-scheme heterojunction photocatalysts based on organic/inorganic coupling.

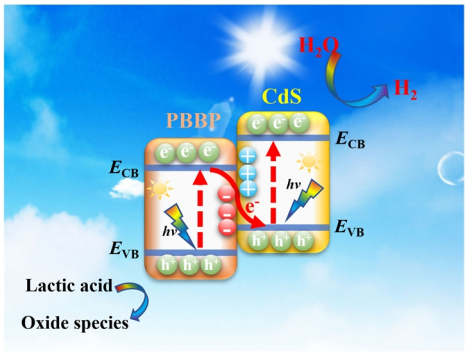

Keywords: photocatalytic hydrogen evolution, pyrene-benzothiadiazole-based conjugated polymers, S-scheme heterojunction, CdS

n INTRODUCTION

Photocatalytic hydrogen evolution from water has attracted great interest because it provides a promising and sustainable technology to solve environmental problems and energy crises.[1-8] Nowadays, conjugated polymers such as g-C_3N_4,[9-13] poly(p-phenylene),[14] triazine-based frameworks,[15] and polybenzothiadiazoles[16,17] have been successfully used in the photocatalytic application. Different from inorganic semiconductors, organic photocatalysts have a delocalized π-system, which benefits from increasing the visible light absorption.[18,19] However, most conjugated polymer semiconductors still exhibit poor separation of photogenerated electron-hole pairs due to their weak built-in fields and amorphous feature with a mass of surface defects.[20,21] To this end, it is still a big challenge for further improving the photocatalytic activity of conjugated polymers.

PBBP-based semiconductor,[21] a new type of conjugated polymers, was successfully used in photocatalytic hydrogen evolution. Pyrene and its derivatives have been widely studied as components of optical probes, sensing systems, and other optoelectronic devices.[22,23] Inspired from the achievements in optoelectronic applications, pyrene-benzothiadiazole-based conjugated polymer is suitable for constructing efficient photocatalysis. So far, most reported pyrene derivatives have been focused on substituting positions 1,3,6,8. Substituting positions 2,7 have been relatively rarely investigated.[24] In fact, the effects of substituents at positions 2,7 on photophysical properties are different from those at positions 1,3,6,8, which result in differences in the energy and intensity of the lowest energy transition.[21] Therefore, it can predict that constructing 2,7-substituted pyrene-benzothiadiazole-based conjugated polymer will bring efficient charge transfer and photocatalytic applications with good photophysical properties.

On the other hand, conjugated polymers have shown good synergy with inorganic semiconductors.[25-30] For instance, covalent organic frameworks (COFs) combined with CdS have great potential for constructing heterojunction photocatalysts due to their strong interfacial interaction.[31-33] S-scheme heterojunction has recently received much attention because of the efficient separation of photogenerated electron-hole pairs and strong redox ability.[34-43] S-scheme charge transport is related to band bending and internal electric field (IEF). The n-type properties and suitable band levels of CdS and PBBP meet the demand for forming an S-scheme PBBP/CdS heterojunction. However, to the best of our knowledge, no studies on photocatalytic H_2 evolution over 2D layered PBBP/CdS heterojunctions have been reported.

Herein, for the first time, we have designed a PBBP/CdS orga-

DOI: 10.14102/j.cnki.0254-5861.2022-0096

nic/inorganic S-scheme semiconductor heterojunction photocatalyst by sonicated methods. PBBP is synthesized via the Suzuki-Miyaura reactions, which shows an appropriate band gap for photocatalytic H_2 evolution. The PBBP/CdS composite shows much better photocatalytic performance and stability than PBBP and CdS. Moreover, ESR and UPS measurement analysis verifies the S-scheme charge transfer pathway and establishes the build-in electric field between CdS and PBBP. The 2D structure enhances the interactions between PBBP and CdS as well as offers sufficient carrier transport channels. Accordingly, the probability of carrier recombination is greatly reduced. This work provides a feasible way for improving the charge separation on PBBP based conjugated polymer.

n RESULTS AND DISCUSSION

Structure and Property Study. Figure 1(b) exhibits the zeta potentials of pure CdS and PBBP, with the latter showing a negative zeta potential of -3.37 mV, and the former exhibiting a positive zeta potential of 5.97 mV. The opposite zeta potentials result in strong electrostatic attraction between PBBP and CdS. The XRD patterns of CdS, PBBP, and PBBP/CdS are depicted in Figure 1(c). Pure PBBP shows a diffraction peak at 23.6°. The other humped peak suggested that PBBP is an amorphous conjugated polymer.[21] Pure CdS shows six district diffraction peaks at 24.95° (100), 26.78° (002), 28.35° (101), 43.88° (110), 48.19° (103), and 52.22° (112), which are indexed as six crystal planes of CdS (PDF#41-1049).[44] The PBBP/CdS composite shows the same district diffraction peaks in Figure 1(c), indicating successful construction of PBBP/CdS. Notably, the diffraction peak at 23.6° disappears in the patterns of PBBP/CdS composite, probably caused by the low content of PBBP and high dispersibility on CdS. In the FT-IR spectroscopy (Figure 1(d)) and ^{13}C NMR spectra of PBBP (Figure 1(e)), the chemical bond and characteristic structure of PBBP could be further confirmed. The ^{13}C NMR spectra of PBBP display the peaks that could be assigned to the phenyl C at 127.35 ppm, while that at 152.77 ppm could be assigned to C=N. As shown in Figure 1(d), the peaks at 1440 and 1603 cm^{-1} could be ascribed to the C=N and N-S bonds.[21] As for the PBBP/CdS composite, the peaks at 1117 and 1003 cm^{-1} can be attributed to the vibration of Cd-S bonds.[45] However, the two extremes of N-S and C=N bonds could not be observed for PBBP/CdS composite. Therefore, the existence of PBBP should be further analyzed by TEM and HRTEM.

TEM and HRTEM images were measured to comprehend the microstructures and morphologies of the PBBP/CdS composite. From Figure 2(a) and 2(b), CdS and PBBP exhibit a typical 2D nanosheet structure. The TEM image of PBBP/CdS composite is shown in Figure 2(c), indicating that CdS nanosheets are uniformly distributed on the surface of PBBP. The HRTEM of CdS and PBBP are shown in Figure S1. Besides, the HRTEM image of PBBP/CdS (Figure 2(d)) shows that the PBBP is loaded on the surface of CdS successfully. The continuous lattice fringes of 0.38

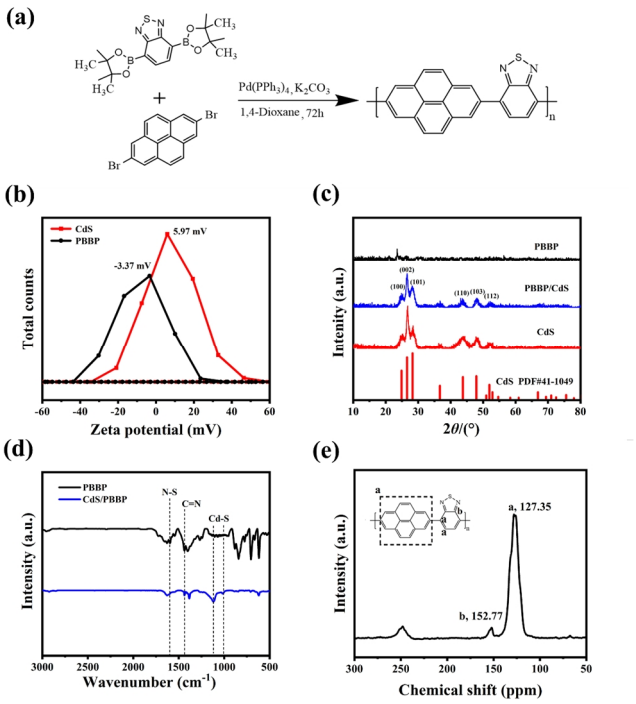

Figure 1. (a) Synthetic route to the pyrene-benzothiadiazole-based conjugated polymer; (b) Zeta potentials of pure CdS and PBBP; (c) XRD patterns of CdS, PBBP, and PBBP/CdS; (d) The FT-IR spectra of PBBP and PBBP/CdS; (e) ^{13}C NMR spectra of the PBBP.

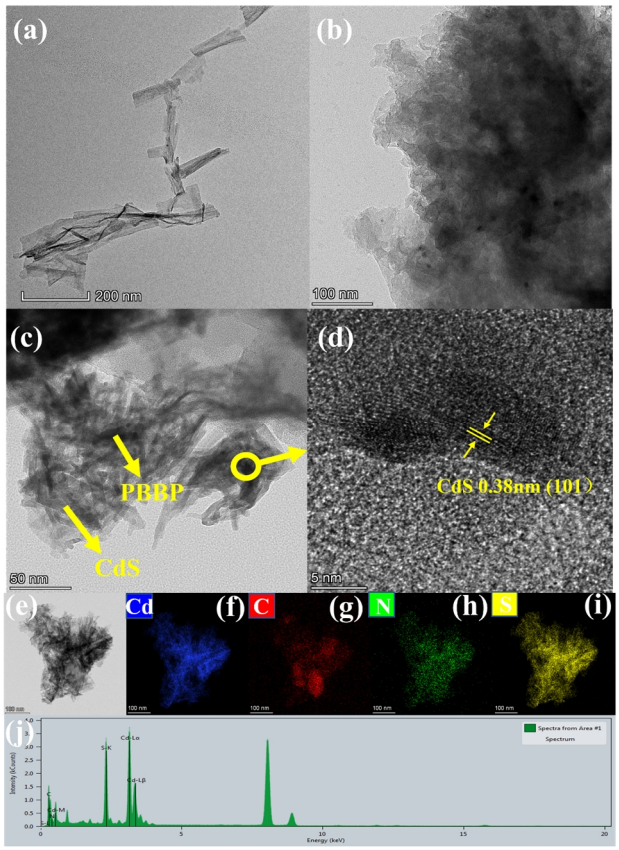

Figure 2. (a) TEM image of CdS; (b) TEM image of PBBP; (c) TEM image of 20% PBBP/CdS; (d) HRTEM image of 20% PBBP/CdS and (e-i) elemental mapping of 20% PBBP/CdS and (j) EDX spectrum of 20% PBBP/CdS.

Chin. J. Struct. Chem. **2022**, 41, 2206031-2206038
DOI: 10.14102/j.cnki.0254-5861.2022-0096

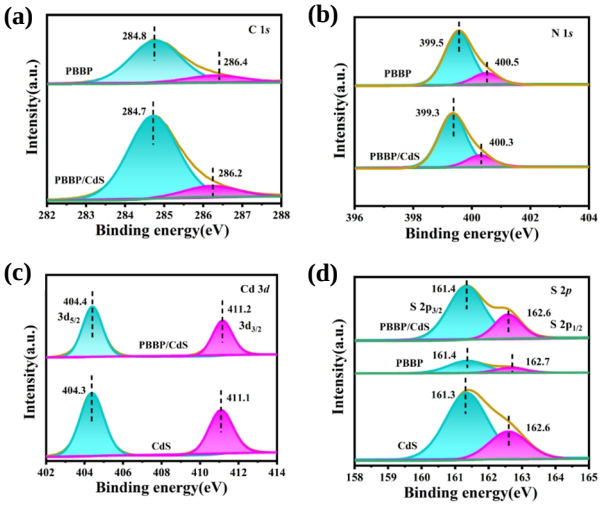

Figure 3. XPS spectra of (a) carbon, (b) nitrogen, (c) cadmium and (d) sulphur.

nm correspond to the (101) plane of CdS.[28,46] Charge transfer is more advantageous due to the close contact between PBBP and CdS. The elemental mapping (Figure 2(e-i)) and EDX spectrum (Figure 2(j)) of 20% PBBP/CdS composite demonstrate the signals of elements corresponding to Cd, C, N and S, which also confirm the uniform distribution of PBBP on CdS.

XPS was used to further confirm the surface properties of PBBP, CdS and PBBP/CdS composite. Figure 3 displays the XPS spectra of the as-prepared photocatalysts. The XPS survey and XPS spectra of PBBP/CdS are depicted in Figure S2. As displayed in Figure 3(a), the C 1s XPS spectra for PBBP can be divided into two peaks at 284.8 and 286.4 eV, attributed to the aromatic sp^2 carbon and the C=N bond, respectively. Two obvious peaks at 399.5 and 400.5 eV could be observed in the N 1s spectrum (Figure 3(b)) due to the existence of C=N and N-S, respectively.[47,48] For pure CdS, two peaks of Cd 3d are located at 404.3 (Cd $3d_{5/2}$) and 411.1 eV (Cd $3d_{3/2}$) (Figure 3(c)). In S 2p XPS spectra (Figure 3(d)), two peaks at 161.3 and 162.6 eV correspond to S $2p_{3/2}$ and S $2p_{1/2}$ of S^{2-}.[49] In the XPS spectrum of PBBP/CdS, signals of C 1s and N 1s are the same as those of pure PBBP. After forming a heterojunction between PBBP and CdS, the binding energies of PBBP/CdS in Figure 3(c) and 3(d) both positively shift by 0.1 eV. Conversely, the binding energies of PBBP/CdS in Figure 3(a) and 3(b) are 0.2 eV negatively shifted compared to PBBP. Such shifts indicate electron transfer from PBBP to CdS due to their different work functions under dark conditions.

Optical Properties and Activities Study. The optical absorption properties of the samples were measured by the UV vis DRS. Both PBBP and CdS exhibit the absorption edge at around 590 and 550 nm in Figure 4(a).[21] The introduction of PBBP enhances the light absorption range for CdS in the visible light area. Therefore, the PBPP/CdS composite has presented a shift of adsorption edge. The photocatalytic hydrogen evolution activity of the as-fabricated photocatalysts was measured in 80 mL lactic acid

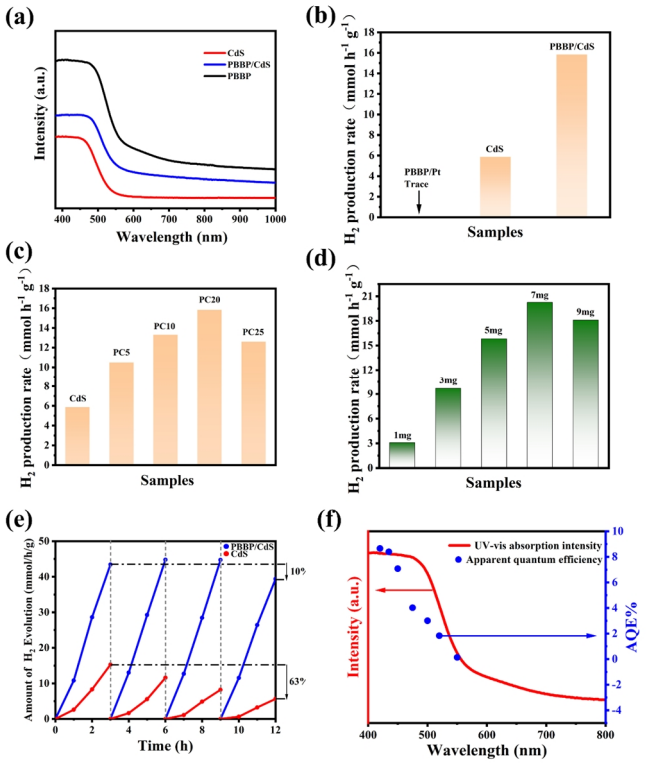

Figure 4. (a) UV-vis diffuse reflection spectra of PBBP, CdS, and PBBP/CdS; (b) The hydrogen evolution of PBBP, CdS, and PBBP/CdS; (c) Comparison of the H_2 evolution rates of PBBP/CdS photocatalysts with different ratios; (d) Comparison of the H_2 evolution rates of PBBP/CdS photocatalysts with different mass; (e) Long-term recycled tests of hydrogen evolution for CdS and PBBP/CdS; (f) Apparent quantum efficiency for PBBP/CdS.

under visible-light irradiation. It could be observed that the H_2 generation rate of CdS is 5.87 mmol h^{-1} g^{-1} from Figure 4(b). In contrast, pure PBBP exhibits poor photocatalytic H_2-evolution performance. Fortunately, the PBBP/CdS composite reaches a noticeable enhancement in photocatalytic H_2 evolution activity (Figure 4(c) and Figure 4(d)). The photocatalytic H_2 production rate of 20% PBBP/CdS gets to 15.83 mmol h^{-1} g^{-1}, which is nearly 2.7 times that of CdS. The enhancement confirms that the formation of S-scheme heterojuction can effectively enhance the photocatalytic performance.[21,50-52]

Long-term cycling tests further investigated the photocatalytic stability of 20% PBBP/CdS under visible-light irradiation. PBBP/CdS composite maintained a high H_2 evolution rate of 14.93 mmol h^{-1} g^{-1} after four reaction cycles. The PBBP/CdS composite kept 90% performance retention, however, it is only 37% for CdS (Figure 4(e)). The photocorrosion of CdS may have caused the decreased photocatalytic performance. The apparent quantum efficiencies of PBBP/CdS at 420, 435, 450, 475, 500, 520 and 550 nm are 8.66%, 8.39%, 7.08%, 4.02%, 3.00%, 1.83% and 0.13%, respectively (Figure 4(f)). These results indicate that forming S-scheme heterojunction is advantageous to enhance the photocatalytic H_2 evolution.

DOI: 10.14102/j.cnki.0254-5861.2022-0096

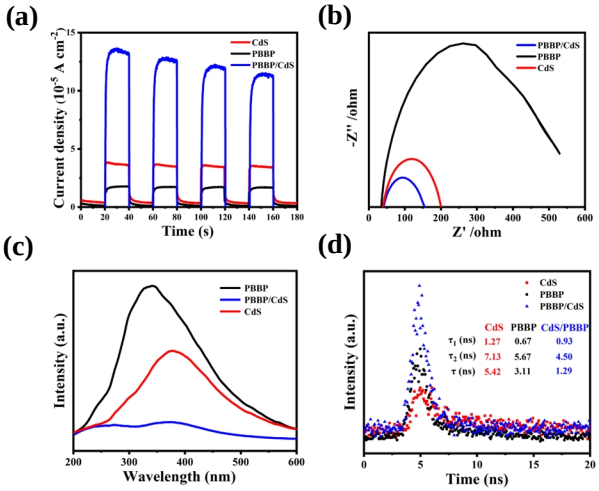

Figure 5. (a) Transient photocurrent response for PBBP, CdS, and 20% PBBP/CdS; (b) Nyquist plots of EIS; (c) PL spectra; (d) Fluorescence lifetime spectrum of CdS, PBBP and PBBP/CdS composite.

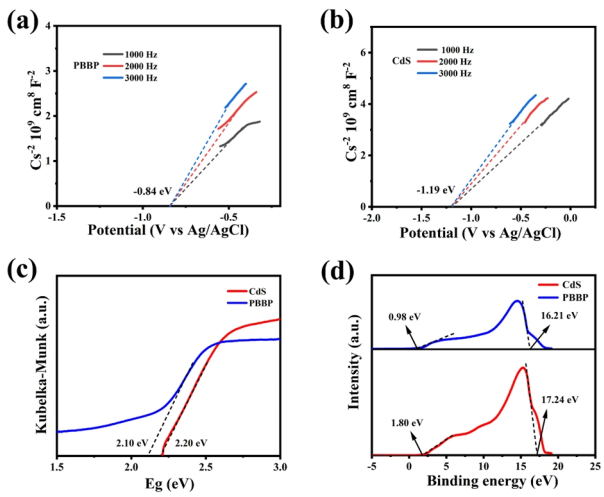

Figure 6. (a) and (b) The Mott-Schottky plot of PBBP and CdS; (c) Kubelka-Munk function *vs*. the energy of incident light plots; (d) UPS spectrum of CdS and PBBP.

Electronic Properties and Study of Mechanism. To further confirm the effective separation of photogenerated electron-hole pairs and accelerated charge transfer in the S-scheme heterojunction, the transient photocurrent-time (i-t) curves were measured (Figure 5(a)). As expected, the 20% PBBP/CdS exhibited a stronger transient photocurrent density than PBBP and CdS, which confirms that loading PBBP on CdS could show a notable improvement in the separation of photoexcited electrons and holes.[26] EIS Nyquist plots (Figure 5(b)) were used to analysize the interfacial charge transfer of the samples. It could be observed that the conductivity of the 20% PBBP/CdS composite is better than those of PBBP and CdS. The smaller radius in the plots, the lower electrical resistance for the samples during the charge transfer process.[25,53,54] Due to the tight interface in 2D/2D PBBP/CdS S-scheme heterojunction, the electrons could effectively transfer between PBBP and CdS. In addition, the overpotential of the 20% PBBP/CdS composite photocatalyst for H_2 evolution was lower than those of PBBP and CdS in the polarization curve (Figure S3). It is noteworthy that the hydrogen-evolution kinetics has been successfully promoted in the system. In a word, constructing the PBBP/CdS S-scheme heterojunction could promote both separation and utilization of photogenerated charges.[55,56]

Photoluminescence (PL, Figure 5(c)) and time resolved photoluminescence (TRPL, Figure 5(d)) were measured to ensure the effective separation of photogenerated electron-hole pairs in PBPP/CdS composite. As shown in Figure 5(c), PBBP displays a strong emission peak compared with CdS and PBBP/CdS composite photocatalyst. The PL intensity of PBPP/CdS was lower than those of PBBP and CdS, revealing effective separation of photogenerated electron-hole pairs in the PBBP/CdS S-scheme heterojunction.[49,57,58] The result of the photoluminescence spectrum is in accord with the discussion mentioned above.

The fitting results of TRPL are shown in Figure 5(d). The short and long lifetime (τ1 and τ2) of pure CdS, PBBP, and 20% PBBP/CdS was respectively estimated to be 1.27, 0.67, 0.93 ns contributed by the radiative pathways and 7.13, 5.67, 4.50 ns reflecting the nonradiative process. Apparently, τ1 and τ2 replace interfacial transfer and recombination of photoexcited eletrons between PBBP and CdS,[25,59,60] respectively. Notably, the τ1 of 20% PBBP/CdS falls between those of PBBP and CdS, respectively, indicating the favorable interfacial electron transfer, while τ2 of 20% PBBP/CdS is shorter than those of neat CdS and PBBP, showing excellent interfacial charge recombination. The average fluorescence lifetime (τ_{ave}) of pure CdS, PBBP, and 20% PBBP/CdS was calculated as 5.42, 3.11, and 1.29 ns, respectively. The 20% PBBP/CdS exhibits the shortest decay time, which not only reflects the better charge separation ability for constructing S-scheme heterojunctions, but also indicates that the photo-induced electrons from PBBP will recombine with the holes of CdS. The result is consistent with the above results and photocatalytic performance. Coupling PBBP with CdS to form the 2D/2D S-scheme heterojunction can also decrease the average fluorescence lifetime and inhibit the recombination of photogenerated carriers in PBBP or CdS.[61,62]

The flat-band potentials (E_{fb}) of PBBP and CdS were evaluated by the Mott Schottky curves at three different frequencies. It can be observed that both PBBP and CdS are n-type semiconductors due to the trend of the curves of C^{-2}-E plots in Figure 6(a) and 6(b). The E_{fb} of CdS and PBBP are -1.19 and -0.84 eV versus Ag/AgCl, respectively. For n-type semiconductors, the flat band potential is usually about 0.1-0.2 eV more positive than the conduction one[26]. Thermodynamically, the enhancement of proton reduction ability is related to the increase of negative conduction band, which is favorable for the generation of H_2.

The Kubelka-Munk function equation can calculate the direct bandgap of CdS and PBBP ($\alpha h\nu = A(h\nu - Eg)^{1/2}$).[28] Figure 6(c) shows the bandgaps of PBBP and CdS are 2.10 and 2.20 eV by the Kubelka-Munk function equation, which is consistent with the values reported in the previous report.[21,63] Moreover, the UPS data could calculate the work function (Φ) and E_{VB} of CdS/PBBP. The UPS spectra of PBBP and CdS are shown in Figure 6(d). The

DOI: 10.14102/j.cnki.0254-5861.2022-0096

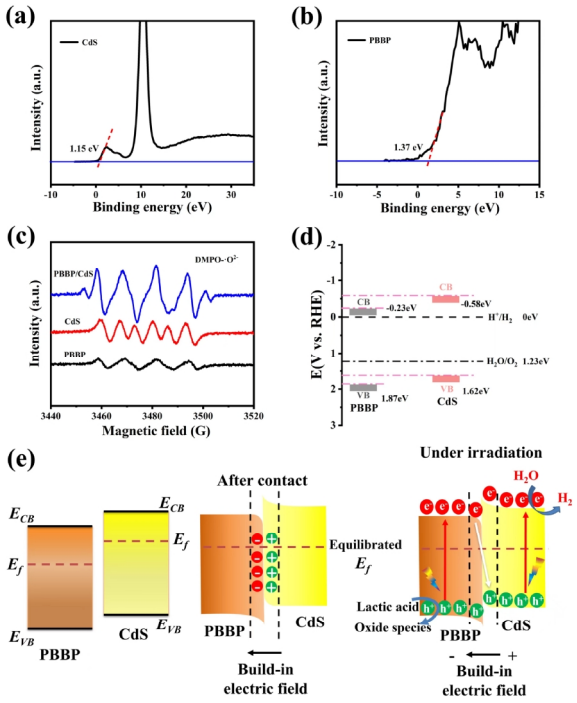

Figure 7. (a) and (b) The valence-band XPS profile of CdS and PBBP; (c) ESR spectra under visible light irradiation; (d) Band structures of PBBP and CdS. (e) The schematic illustration of interfacial electron transfer, E_f equilibrium, and migration of photogenerated carriers in PBBP/CdS S-scheme heterojunction under illumination.

*Φ*s of PBBP and CdS are 5.01 and 3.98 eV, respectively.[64] Therefore, the E_{VB} of PBBP and CdS are 5.99 and 5.78 eV, respectively. It is well known that E_{CB} and E_{VB} need unit conversions (E_{RHE} = E_{NHE} + 0.0591*pH (pH = 7)). For this reason, the values of E_{VB} and E_{CB} for PBBP were calculated to be 1.96 and -0.14 eV (*vs*. RHE). Using the same calculation for CdS, the results can be obtained for E_{VB} as 1.75 eV and E_{CB} as -0.45 eV. It can be confirmed that a built-in electric field is established between PBBP and CdS. We used UPS to determine the *Φ*s of PBBP and CdS, as well as to confirm the formation of S-scheme heterojunction.

In addition, the valence band X-ray photoelectron spectroscopy (VB-XPS) and ESR were measured. As Figure 7(a) and 7(b) revealed, the VB positions of CdS and PBBP are located at 1.15 and 1.37 eV (*vs*. NHE), respectively. Therefore, the VB and CB positions of PBBP can be calculated as 1.84 and -0.26 eV (*vs*. RHE), respectively. Using the same calculation for CdS, the results can be obtained for VB as 1.62 eV and CB as -0.58 eV (*vs*. RHE). ESR has further verified the formation of S-scheme heterojunctions between CdS and PBBP, DMPO was used as the capture agent for $•O^{2-}$. As shown in Figure S4, no ESR signals can be seen in the dark for all samples. As displayed in Figure 7(c), the characteristic peaks of DMPO-$•O^{2-}$ can be monitored for pure CdS, PBBP, and PBBP/CdS under visible light irradiation, suggesting the generation of $•O^{2-}$ in the reaction system.[65] The result indicates that photogenerated electrons are accumulated on the CB of CdS under visible light irradiation. The electrons on the CB of PBBP recombine with the holes on the VB of CdS, which verifies the successful formation of S-scheme heterojunction.[38,66-68] Combing the bandgap and Mott-Schottky results, the E_{VB} potentials are 1.87 eV for PBBP and 1.62 eV for CdS. More clearly, the estimated E_{CB} and E_{VB} for the photocatalysts are displayed in Figure 7(d), and the schematic illustration of band structures from the results of UPS and VB-XPS are shown in Figure S5 and S6.

The above experimental results showed that both PBBP and CdS have matched energy band structures, which is advantageous for the successful formation of S-scheme heterojunction. Photogenerated electrons on the surface of PBBP will transfer to the VB of CdS nanosheets and then recombine with the holes under visible light irradiation. As illustrated in Figure 7(e), PBBP displays more positive band positions and Fermi level than CdS. After loading PBBP on the surface of CdS, the free electrons in CdS will readily transfer to PBBP across the interface until Fermi levels reach equilibrium. For PBBP, the electrons are accumulated on the interface. Thus, the electron density in CdS decreases. As a result, the bands of PBBP and CdS will bend downward and upward, respectivly. Therefore, a built-in electric field is established. Under irradiation, the electrons in CdS and PBBP are photoexcited from VB to CB, respectively. Then the photogenerated electrons in PBBP consume the holes in CdS, which leaves photogenerated holes in VB of PBBP as well as electrons in CB of CdS, respectively. The path of charge transfer follows the step-scheme route.[25,69]

n CONCLUSIONS

In summary, a pyrene-benzothiadiazole-based conjugated polymers organic/inorganic S-scheme heterojunction photocatalyst is prepared by mixing CdS with PBBP through the ultrasonic mixing method. The S-scheme heterojunction and the establishment of built-in electric field between CdS and PBBP are systematically investigated by ESR and UPS. Compared with CdS, the PBBP/CdS composite exhibits better optical properties, higher H_2 evolution and more efficient capability of electron-holes separation. The maximum photocatalytic H_2 evolution rate of 20% PBBP/CdS reaches 15.83 mmol $h^{-1}g^{-1}$ without any cocatalyst, nearly 2.7 times higher than CdS. The apparent quantum efficiency of the 20% PBBP/CdS achieves 8.66% at 420 nm. Experiment results indicate that PBBP/CdS S-scheme heterojunction can effectively separate photogenerated electron-hole pairs, accelerate carriers transfer and improve redox ability. This work highlights the great importance of pyrene-benzothiadiazole-based conjugated polymer in constructing organic/inorganic S-scheme heterojunction photocatalyst for improving photocatalytic performance.

n EXPERIMENTAL SECTIONS

All the chemicals were analytically pure, purchased from Shanghai Macklin and Aladdin Reagent Co. Ltd. The pyrene-benzothiadiazole-based conjugated polymer preparation process is shown in Figure 1(a). The details of characterizations, photocatalytic hydrogen evolution and electrochemical measurements are given in the ESI.

Preparation of CdS. Firstly, 0.617 g of cadmium nitrate ($Cd(NO_3)_2$) and 0.4567 g thiourea (CH_4N_2S) were dissolved in 60 mL of EDA. Then, the solution was heated at 100 °C for 8 h. After

DOI: 10.14102/j.cnki.0254-5861.2022-0096

cooling to room temperature, the obtained yellow products were washed by ethanol and ultra pure water repeatedly.

Preparation of PBBP. 57.14 mg of 4,7-bis(4,4,5,5-tetramethyl-1,3,2-dioxaborolan-2-yl)-2,1,3-benzothiadiazole, 100 mg of 2,7-dibromopyrene and 17.14 mg of $Pd(PPh_3)_4$(0) were mixed with 1,4-dioxane (DMF) and K_2CO_3 (2.0 M, 2.4 mL) in the polymerization. Then the mixture was stirred at 100 ℃ for 72 h under Ar atmosphere[21]. After cooling to room temperature, the mixture was washed with ultra-pure water, methanol, and tetrahydrofuran to remove oligomers and Pd residues.

Synthesis of the PBBP/CdS Composite Photocatalysts. 20 mg CdS and 4 mg PBBP were added into 30 mL of ethanol, then the mixture was sonicated and stirred for 1 h, respectively. Subsequently, the ethanol was evaporated at 60 °C to gain the target product. By varying the amount of PBBP to be 1, 2, and 5 mg, the samples of CPx were obtained (x = 5, 10, or 25, where x is the theoretical weight percentage of PBBP concerning CdS).

n ACKNOWLEDGEMENTS

X.L. thanks the National Natural Science Foundation of China (21975084, 51672089) and Natural Science Foundation of Guangdong Province (2021A1515010075) for their support.

n AUTHOR INFORMATION

Corresponding authors. Emails: Xinli@scau.edu.cn(X. Li) and shenrongchenscau@163.com (R. Shen)

n AUTHOR CONTRIBUTION

+ These authors contributed equally to this work

n COMPETING INTERESTS

The authors declare no competing interests.

n ADDITIONAL INFORMATION

Supplementary information is available for this paper at http://manu30.magtech.com.cn/jghx/EN/10.14102/j.cnki.0254-5861.2022-0096

For submission: https://mc03.manuscriptcentral.com/cjsc

n REFERENCES

(1) Wang, H.; Li, X.; Zhao, X.; Li, C.; Song, X.; Zhang, P.; Huo, P.; Li, X. A review on heterogeneous photocatalysis for environmental remediation: from semiconductors to modification strategies. *Chin. J. Catal.* **2022**, 43, 178-214.

(2) Liu, Y.; Niu, H.; Gu, W.; Cai, X.; Mao, B.; Li, D.; Shi, W. In-situ construction of hierarchical CdS/MoS_2 microboxes for enhanced visible-light photocatalytic H_2 production. *Chem. Eng. J.* **2018**, 339, 117-124.

(3) Sun, B.; Qiu, P.; Liang, Z.; Xue, Y.; Zhang, X.; Yang, L.; Cui, H.; Tian, J. The fabrication of 1D/2D CdS nanorod@Ti_3C_2 MXene composites for good photocatalytic activity of hydrogen generation and ammonia synthesis. *Chem. Eng. J.* **2021**, 406, 127177.

(4) Sayed, M.; Yu, J.; Liu, G.; Jaroniec, M. Non-noble plasmonic metal-based photocatalysts. *Chem. Rev.* **2022**, DOI:10.1021/acs.chemrev.1c00473.

(5) Gao, D.; Xu, J.; Wang, L.; Zhu, B.; Yu, H.; Yu, J. Optimizing atomic hydrogen desorption of sulfur-rich NiS_{1+x} cocatalyst for boosting photocatalytic H_2 evolution. *Adv. Mater.* **2022**, 34, 2108475.

(6) Shen, R.; Hao, L.; Chen, Q.; Zheng, Q.; Zhang, P.; Li, X. P-Doped g-C_3N_4 nanosheets with highly dispersed $Co_{0.2}N_{1.6}Fe_{0.2}P$ cocatalyst for efficient photocatalytic hydrogen evolution. *Acta Phys-Chim. Sin.* **2021**, 0, 2110014.

(7) Xu, C. S.; Lv, P. W. Photo-assisted deposited titanium dioxide film and the enhancement of its photocatalytic water splitting activity. *Chin. J. Struct. Chem.* **2021**, 40, 1223-1230.

(8) Jiang, X.; Chen, Y. X.; Lu, C. Z. Bio-inspired materials for photocatalytic hydrogen production. *Chin. J. Struct. Chem.* **2020**, 39, 2123-2130.

(9) Fan, Z.; Guo, X.; Jin, Z.; Li, X.; Li, Y. Bridging effect of S-C bond for boosting electron transfer over cubic hollow CoS/g-C_3N_4 heterojunction toward photocatalytic hydrogen production. *Langmuir* **2022**, 38, 3244-3256.

(10) Yang, M.; Wang, P.; Li, Y.; Tang, S.; Lin, X.; Zhang, H.; Zhu, Z.; Chen, F. Graphene aerogel-based NiAl-LDH/g-C_3N_4 with ultratight sheet-sheet heterojunction for excellent visible-light photocatalytic activity of CO_2 reduction. *Appl. Catal. B-Environ.* **2022**, 306, 121065.

(11) Wen, J.; Xie, J.; Chen, X.; Li, X. A review on g-C_3N_4-based photocatalysts. *Appl. Surf. Sci.* **2017**, 391, 72-123.

(12) Li, Y.; Li, X.; Zhang, H. W.; Fan, J. J.; Xiang, Q. J. Design and application of active sites in g-C_3N_4-based photocatalysts. *J. Mater. Sci. Technol.* **2020**, 56, 69-88.

(13) Li, Y. F.; Zhou, M. H.; Cheng, B.; Shao, Y. Recent advances in g-C_3N_4-based heterojunction photocatalysts. *J. Mater. Sci. Technol.* **2020**, 56, 1-17.

(14) Sprick, R. S.; Bonillo, B.; Clowes, R.; Guiglion, P.; Brownbill, N. J.; Slater, B. J.; Blanc, F.; Zwijnenburg, M. A.; Adams, D. J.; Cooper, A. I. Visible-light-driven hydrogen evolution using planarized conjugated polymer photocatalysts. *Angew. Chem. Int. Ed.* **2016**, 128, 1824-1828.

(15) Kuecken, S.; Acharjya, A.; Zhi, L.; Schwarze, M.; Schomacker, R.; Thomas, A. Fast tuning of covalent triazine frameworks for photocatalytic hydrogen evolution. *Chem. Commun.* **2017**, 53, 5854-5857.

(16) Yang, C.; Ma, B. C.; Zhang, L.; Lin, S.; Ghasimi, S.; Landfester, K.; Zhang, K. A.; Wang, X. Molecular engineering of conjugated polybenzothiadiazoles for enhanced hydrogen production by photosynthesis. *Angew. Chem. Int. Ed.* **2016**, 55, 9202-9206.

(17) Xu, Y.; Mao, N.; Zhang, C.; Wang, X.; Zeng, J.; Chen, Y.; Wang, F.; Jiang, J.-X. Rational design of donor-π-acceptor conjugated microporous polymers for photocatalytic hydrogen production. *Appl. Catal. B-Environ.* **2018**, 228, 1-9.

(18) Liu, C.; Wang, K.; Gong, X.; Heeger, A. J. Low bandgap semiconducting polymers for polymeric photovoltaics. *Chem. Soc. Rev.* **2016**, 45, 4825-4846.

(19) Kang, H.; Lee, W.; Oh, J.; Kim, T.; Lee, C.; Kim, B. J. From fullerene-polymer to all-polymer solar cells: the importance of molecular packing, orientation, and morphology control. *Accounts Chem. Res.* **2016**, 49, 2424-2434.

(20) Sachs, M.; Sprick, R. S.; Pearce, D.; Hillman, S. A. J.; Monti, A.; Guilbert, A. A. Y.; Brownbill, N. J.; Dimitrov, S.; Shi, X.; Blanc, F.; Zwijnenburg, M. A.; Nelson, J.; Durrant, J. R.; Cooper, A. I. Understanding structure-activity relationships in linear polymer photocatalysts for hydrogen evolution. *Nat. Commun.* **2018**, 9, 4968.

(21) Cheng, C.; Wang, X.; Lin, Y.; He, L.; Jiang, J.-X.; Xu, Y.; Wang, F. The effect of molecular structure and fluorination on the properties of pyrene-benzothiadiazole-based conjugated polymers for visible-light-driven hy-

drogen evolution. *Polym. Chem-UK.* **2018**, 9, 4468-4475.
(22) Figueira-Duarte, T. M.; Mullen, K. Pyrene-based materials for organic electronics. *Chem. Rev.* **2011**, 111, 7260-7314.
(23) Pandey, M. D.; Mishra, A. K.; Chandrasekhar, V.; Verma, S. Silver-guided excimer emission in an adenine-pyrene conjugate: fluorescence lifetime and crystal studies. *Inorg. Chem.* **2010**, 49, 2020-2022.
(24) Sprick, R. S.; Jiang, J. X.; Bonillo, B.; Ren, S.; Ratvijitvech, T.; Guiglion, P.; Zwijnenburg, M. A.; Adams, D. J.; Cooper, A. I. Tunable organic photocatalysts for visible-light-driven hydrogen evolution. *J. Am. Chem. Soc.* **2015**, 137, 3265-3270.
(25) Cheng, C.; He, B.; Fan, J.; Cheng, B.; Cao, S.; Yu, J. An inorganic/organic S-scheme heterojunction H_2-production photocatalyst and its charge transfer mechanism. *Adv. Mater.* **2021**, 33, 2100317.
(26) Hu, Y.; Hao, X.; Cui, Z.; Zhou, J.; Chu, S.; Wang, Y.; Zou, Z. Enhanced photocarrier separation in conjugated polymer engineered CdS for direct Z-scheme photocatalytic hydrogen evolution. *Appl. Catal. B-Environ.* **2020**, 260, 118131.
(27) Shen, R.; Ren, D.; Ding, Y.; Guan, Y.; Ng, Y. H.; Zhang, P.; Li, X. Nanostructured CdS for efficient photocatalytic H_2 evolution: a review. *Sci. China Mater.* **2020**, 63, 2153-2188.
(28) Bai, J.; Shen, R.; Jiang, Z.; Zhang, P.; Li, Y.; Li, X. Integration of 2D layered CdS/WO_3 S-scheme heterojunctions and metallic Ti_3C_2 MXene-based Ohmic junctions for effective photocatalytic H_2 generation. *Chin. J. Catal.* **2022**, 43, 359-369.
(29) Han, G.; Xu, F.; Cheng, B.; Li, Y.; Yu, J.; Zhang, L. Enhanced photocatalytic H_2O_2 production over inverse opal ZnO@ polydopamine s-scheme heterojunctions. *Acta Phys-Chim. Sin.* **2022**, 38, 2112037.
(30) Ma, X. W.; Lin, H. F.; Li, Y. Y.; Wang, L.; Pu, X. P.; Yi, X. J. Dramatically enhanced visible-light-responsive H_2 evolution of $Cd_{1-x}Zn_xS$ via the synergistic effect of Ni_2P and 1T/2H MoS_2 cocatalysts. *Chin. J. Struct. Chem.* **2021**, 40, 7-22.
(31) Wang, D.; Zeng, H.; Xiong, X.; Wu, M.-F.; Xia, M.; Xie, M.; Zou, J.-P.; Luo, S.-L. Highly efficient charge transfer in CdS-covalent organic framework nanocomposites for stable photocatalytic hydrogen evolution under visible light. *Sci. Bull.* **2020**, 65, 113-122.
(32) Wang, D.; Li, X.; Zheng, L. L.; Qin, L. M.; Li, S.; Ye, P.; Li, Y.; Zou, J. P. Size-controlled synthesis of CdS nanoparticles confined on covalent triazine-based frameworks for durable photocatalytic hydrogen evolution under visible light. *Nanoscale* **2018**, 10, 19509-19516.
(33) Tang, S.; Xia, Y.; Fan, J.; Cheng, B.; Yu, J.; Ho, W. Enhanced photocatalytic H_2 production performance of CdS hollow spheres using C and Pt as bi-cocatalysts. *Chin. J. Catal.* **2021**, 42, 743-752.
(34) Huang, Y.; Mei, F.; Zhang, J.; Dai, K.; Dawson, G. Construction of 1D/2D $W_{18}O_{49}$/porous g-C_3N_4 S-scheme heterojunction with enhanced photocatalytic H_2 evolution. *Acta Phys-Chim. Sin.* **2022**, 38, 2108028.
(35) Zhang, L.; Zhang, J.; Yu, H.; Yu, J. Emerging S-scheme photocatalyst. *Adv. Mater.* **2022**, 34, 2107668.
(36) Xu, Q.; Zhang, L.; Cheng, B.; Fan, J.; Yu, J. S-scheme heterojunction photocatalyst. *Chem* **2020**, 6, 1543-1559.
(37) Wageh, S.; Al-Ghamdi, A. A.; Jafer, R.; Li, X.; Zhangc, P. A new heterojunction in photocatalysis: S-scheme heterojunction. *Chin. J. Catal.* **2021**, 42, 667-669.
(38) Li, S.; Cai, M.; Liu, Y.; Zhang, J.; Wang, C.; Zang, S.; Zhang, P.; Li, X.; Li, Y. In-situ constructing C_3N_5 nanosheets/Bi_2WO_6 nanodots S-scheme heterojunction with enhanced structural defects for efficiently photocatalytic removal of tetracycline and Cr(VI). *Inorg. Chem. Front.* **2022**, doi: 10.1039/D2QI00317A.
(39) Bai, J.; Chen, W.; Shen, R.; Jiang, Z.; Zhang, P.; Liu, W.; Li, X. Regulating interfacial morphology and charge-carrier utilization of Ti_3C_2 modified all-sulfide CdS/$ZnIn_2S_4$ S-scheme heterojunctions for effective photocatalytic H_2 evolution. *J. Mater. Sci. Technol.* **2022**, 112, 85-95.
(40) Dai, M.; He, Z.; Zhang, P.; Li, X.; Wang, S. $ZnWO_4$-$ZnIn_2S_4$ S-scheme heterojunction for enhanced photocatalytic H_2 evolution. *J. Mater. Sci. Technol.* **2022**, 122, 231-242.
(41) Jiang, J.; Xiong, Z.; Wang, H.; Liao, G.; Bai, S.; Zou, J.; Wu, P.; Zhang, P.; Li, X. Sulfur-doped g-C_3N_4/g-C_3N_4 isotype step-scheme heterojunction for photocatalytic H_2 evolution. *J. Mater. Sci. Technol.* **2022**, 118, 15-24.
(42) Xu, Q.; Wageh, S.; Al-Ghamdi, A. A.; Li, X. Design principle of S-scheme heterojunction photocatalyst. *J. Mater. Sci. Technol.* **2022**, 124, 171-173.
(43) Xu, F.; Meng, K.; Cheng, B.; Wang, S.; Xu, J.; Yu, J. Unique S-scheme heterojunctions in self-assembled TiO_2/$CsPbBr_3$ hybrids for CO_2 photoreduction. *Nat. Commun.* **2020**, 11, 4613.
(44) Deka, K.; Kalita, M. P. C. Evidence of reaction rate influencing cubic and hexagonal phase formation process in CdS nanocrystals. *Chem. Phys. Lett.* **2016**, 652, 11-15.
(45) Ai, L.; Su, J.; Wang, M.; Jiang, J. Bamboo-structured nitrogen-doped carbon nanotube coencapsulating cobalt and molybdenum carbide nanoparticles: an efficient bifunctional electrocatalyst for overall water splitting. *ACS Sustain. Chem. Eng.* **2018**, 6, 9912-9920.
(46) Ren, D.; Shen, R.; Jiang, Z.; Lu, X.; Li, X. Highly efficient visible-light photocatalytic H_2 evolution over 2D-2D CdS/Cu_7S_4 layered heterojunctions. *Chin. J. Catal.* **2020**, 41, 31-40.
(47) Zhou, J.; Lei, Y.; Ma, C.; Lv, W.; Li, N.; Wang, Y.; Xu, H.; Zou, Z. A (001) dominated conjugated polymer with high-performance of hydrogen evolution under solar light irradiation. *Chem. Commun.* **2017**, *53*, 10536-10539.
(48) Jin, Z.; Zhang, L.; Wang, G.; Li, Y.; Wang, Y. Graphdiyne formed a novel CuI-GD/g-C_3N_4 S-scheme heterojunction composite for efficient photocatalytic hydrogen evolution. *Sustain. Energy Fuels* **2020**, 4, 5088-5101.
(49) Shen, R.; Ding, Y.; Li, S.; Zhang, P.; Xiang, Q.; Ng, Y. H.; Li, X. Constructing low-cost Ni_3C/twin-crystal $Zn_{0.5}Cd_{0.5}S$ heterojunction/homojunction nanohybrids for efficient photocatalytic H_2 evolution. *Chin. J. Catal.* **2021**, 42, 25-36.
(50) Zhang, X.-H.; Wang, X.-P.; Xiao, J.; Wang, S.-Y.; Huang, D.-K.; Ding, X.; Xiang, Y.-G.; Chen, H. Synthesis of 1,4-diethynylbenzene-based conjugated polymer photocatalysts and their enhanced visible/near-infrared-light-driven hydrogen production activity. *J. Catal.* **2017**, 350, 64-71.
(51) Sprick, R. S.; Bonillo, B.; Sachs, M.; Clowes, R.; Durrant, J. R.; Adams, D. J.; Cooper, A. I. Extended conjugated microporous polymers for photocatalytic hydrogen evolution from water. *Chem. Commun.* **2016**, 52, 10008-10011.
(52) Sun, L.; Li, L.; Yang, J.; Fan, J.; Xu, Q. Fabricating covalent organic framework/CdS S-scheme heterojunctions for improved solar hydrogen generation. *Chin. J. Catal.* **2022**, 43, 350-358.
(53) He, K.; Xie, J.; Liu, Z.-Q.; Li, N.; Chen, X.; Hu, J.; Li, X. Multi-functional Ni_3C cocatalyst/g-C_3N_4 nanoheterojunctions for robust photocatalytic H_2 evolution under visible light. *J. Mater. Chem. A* **2018**, 6, 13110-13122.
(54) Wen, J.; Xie, J.; Zhang, H.; Zhang, A.; Liu, Y.; Chen, X.; Li, X. Constructing multifunctional metallic Ni interface layers in the g-C_3N_4 nanosheets/amorphous NiS heterojunctions for efficient photocatalytic H_2 gene-

DOI: 10.14102/j.cnki.0254-5861.2022-0096

ration. *ACS Appl. Mater. Inter.* **2017**, 9, 14031-14042.
(55) Hu, T.; Li, P.; Zhang, J.; Liang, C.; Dai, K. Highly efficient direct Z-scheme WO_3/CdS-diethylenetriamine photocatalyst and its enhanced photocatalytic H_2 evolution under visible light irradiation. *Appl. Surf. Sci.* **2018**, 442, 20-29.
(56) Wageh, S.; Al-Ghamdi, A. A.; Al-Hartomy, O. A.; Alotaibi, M. F.; Wang, L. CdS/polymer S-scheme H_2-production photocatalyst and its in-situ irradiated electron transfer mechanism. *Chin. J. Catal.* **2022**, 43, 586-588.
(57) Bai, J.; Shen, R.; Chen, W.; Xie, J.; Zhang, P.; Jiang, Z.; Li, X. Enhanced photocatalytic H_2 evolution based on a $Ti_3C_2/Zn_{0.7}Cd_{0.3}S/Fe_2O_3$ Ohmic/S-scheme hybrid heterojunction with cascade 2D coupling interfaces. *Chem. Eng. J.* **2022**, 429, 132587.
(58) Shen, R.; He, K.; Zhang, A.; Li, N.; Ng, Y. H.; Zhang, P.; Hu, J.; Li, X. In-situ construction of metallic Ni_3C@Ni core-shell cocatalysts over g-C_3N_4 nanosheets for shell-thickness-dependent photocatalytic H_2 production. *Appl. Catal. B-Environ.* **2021**, 291, 120104.
(59) Xia, P.; Cao, S.; Zhu, B.; Liu, M.; Shi, M.; Yu, J.; Zhang, Y. Designing a 0D/2D S-scheme heterojunction over polymeric carbon nitride for visible-light photocatalytic inactivation of bacteria. *Angew. Chem. Int. Ed.* **2020**, 59, 5218-5225.
(60) Luo, J.; Lin, Z.; Zhao, Y.; Jiang, S.; Song, S. The embedded $CuInS_2$ into hollow-concave carbon nitride for photocatalytic H_2O splitting into H_2 with S-scheme principle. *Chin. J. Catal.* **2020**, 41, 122-130.
(61) Shen, R.; Lu, X.; Zheng, Q.; Chen, Q.; Ng, Y. H.; Zhang, P.; Li, X. Tracking S-scheme charge transfer pathways in Mo_2C/CdS H_2-evolution photocatalysts. *Solar RRL* **2021**, 5, 2100177.
(62) Shi, R.; Cao, Y.; Bao, Y.; Zhao, Y.; Waterhouse, G. I. N.; Fang, Z.; Wu, L. Z.; Tung, C. H.; Yin, Y.; Zhang, T. Self-assembled Au/CdSe nanocrystal clusters for plasmon-mediated photocatalytic hydrogen evolution. *Adv. Mater.* **2017**, 29, 1700803.
(63) Ren, D.; Liang, Z.; Ng, Y. H.; Zhang, P.; Xiang, Q.; Li, X. Strongly coupled 2D-2D nanojunctions between P-doped Ni_2S (Ni_2SP) cocatalysts and CdS nanosheets for efficient photocatalytic H_2 evolution. *Chem. Eng. J.* **2020**, 390, 124496.
(64) Jiang, Z.; Chen, Q.; Zheng, Q.; Shen, R.; Zhang, P.; Li, X. Constructing 1D/2D schottky-based heterojunctions between $Mn_{0.2}Cd_{0.8}S$ nanorods and Ti_3C_2 nanosheets for boosted photocatalytic H_2 evolution. *Acta Phys-Chim. Sin.* **2021**, 37, 2010059.
(65) Zhao, Z.; Shen, B.; Hu, Z.; Zhang, J.; He, C.; Yao, Y.; Guo, S. Q.; Dong, F. Recycling of spent alkaline Zn-Mn batteries directly: combination with TiO_2 to construct a novel Z-scheme photocatalytic system. *J. Hazard. Mater.* **2020**, 400, 123236.
(66) Li, X. B.; Liu, J. Y.; Huang, J. T.; He, C. Z.; Feng, Z. J.; Chen, Z.; Wan, L. Y.; Deng, F. All organic S-scheme heterojunction PDI-Ala/S-C_3N_4 photocatalyst with enhanced photocatalytic performance. *Acta Phys-Chim. Sin.* **2021**, 37, 2010030.
(67) Li, X.; Luo, Q.; Han, L.; Deng, F.; Yang, Y.; Dong, F. Enhanced photocatalytic degradation and H_2 evolution performance of NCDs/S-C_3N_4 S-scheme heterojunction constructed by π-π conjugate self-assembly. *J. Mater. Sci. Technol.* **2022**, 114, 222-232.
(68) Li, X. B.; Kang, B. B.; Dong, F.; Zhang, Z. Q.; Luo, X. D.; Han, L.; Huang, J. T.; Feng, Z. J.; Chen, Z.; Xu, J. L.; Peng, B. L.; Wang, Z. L. Enhanced photocatalytic degradation and H_2/H_2O_2 production performance of S-pCN/$WO_{2.72}$ S-scheme heterojunction with appropriate surface oxygen vacancies. *Nano Energy* **2021**, 81, 105671.
(69) Li, S.; Wang, C.; Cai, M.; Yang, F.; Liu, Y.; Chen, J.; Zhang, P.; Li, X.; Chen, X. Facile fabrication of TaON/Bi_2MoO_6 core-shell S-scheme heterojunction nanofibers for boosting visible-light catalytic levofloxacin degradation and Cr(VI) reduction. *Chem. Eng. J.* **2022**, 428, 131158.

Received: April 27, 2022
Accepted: May 18, 2022
Published: June 20, 2022

DOI: 10.14102/j.cnki.0254-5861.2022-0096